Third harmonic generation due to free carrier in InSb using terahertz free electron laser

Thanh Nhat Khoa Phan,[1] Shimizu Tomoki,[1] You Wei Wang,[1] Kosaku Kato,[1] Verdad C. Agulto,[1] Goro Isoyama,[2] Shinsuke Fujioka,[1] and Makoto Nakajima[1,*]

[1]*Institute of Laser Engineering, Osaka University, 2-6 Yamadaoka, Suita, Osaka 565-0871, Japan*
[2]*SANKEN (Institute of Science and Industrial Research), Osaka University, 8-1 Mihogaoka, Ibaraki, Osaka 567-0047, Japan*
* nakajima.makoto.ile@osaka-u.ac.jp

Received XX Month XXXX; revised XX Month, XXXX; accepted XX Month XXXX; posted XX Month XXXX (Doc. ID XXXXX); published XX Month XXXX

We report the third harmonic generation (THG) in InSb semiconductor irradiated by a terahertz (THz) free electron laser (FEL). The conversion of 4 THz (wavelength 70 µm) FEL outputs into its third harmonic 12 THz was observed. We found that by tuning the sample temperature to 360 K, a high conversion efficiency up to 1% can be obtained and is the highest in the THz and FIR regions below 10 THz. We also discuss the observed intensity dependence of THG with the nonlinear order lower than 3 when the pumping intensity was high.

During the last few decades, the science of researching physics phenomena in the terahertz (THz) frequency range has experienced a profound transformation, from being only an emerging trend to a well-established technology. It has found vast applications in both fundamental science and practical application [1–10]. To further expand the capability of THz technologies, nonlinear phenomena in the THz region have received much interest so far. However, the research advances have been less than that of the optical region, mainly because of the relatively weak output power of conventional tabletop THz sources. To investigate nonlinear phenomena in THz range, use of a THz free electron laser (FEL) [11–17] is one of the most powerful ways. The merits of an FEL include strong pulse energy (tens of mJ), narrow bandwidth, high coherence, short pulse duration and tunable wavelength. Owing to these merits, FELs have been widely applied in studying various topics, including switching the state of phase change memory material [18,19], controlling spin state in magnetic material [20,21], to name a few.

Among various nonlinear phenomena induced by intense electromagnetic wave, the harmonic generation is the most basic one, and has many promising applications, such as high resolution microscopy [22] or characterizing ultrashort laser pulse [23]. The harmonic generation in THz region has been studied by several authors [24–32]. For example, it was recently reported that materials with massless Dirac fermions such as graphene [26] and topological insulators (TI) [25,30] shows high efficiency of harmonic generation due to the linearity of band structures. The efficiency was enhanced by the use of metamaterial [25] or quantum well structure [30]. With the intense FEL, research on THz harmonic generation enters the nonperturbative regime where not only surprising efficiency but also various other nonlinear physics can be observed. For example, the impact ionization, tunneling ionization, and phonon emission were discussed based on the harmonic generation of THz-FEL output in boron-doped silicon [31,32]. On the other hand, the free electron motion in usual undoped bulk semiconductors can also induce nonlinear polarization due to the nonparabolicity of the band structure [33]. This can be understood intuitively as follows. The effective mass of a free electron m^* is the inverse of the second derivative of the energy-momentum dispersion relation $E(p)$ by the crystal momentum p : $1/m^* = \partial^2 E/\partial p^2$. Since $E(p) \propto p^2$ (parabolic band structure) is not strictly accurate, m^* becomes a function of p. This dependence of m^* on p (nonparabolicity) causes the nonlinear response of electron motion to an electric field, resulting in the harmonic generation. According to the theory [33], the third-order nonlinear susceptibility due to the nonparabolicity of the conduction band $\chi^{(3)}$ is estimated as:

$$\chi^{(3)} \propto \frac{n_e}{(m^*)^2 E_G \omega_f^4} \cdot \frac{1 + 8E_F/5E_G}{(1 + 4E_F/E_G)^{5/2}}, \qquad (1)$$

where n_e, E_F, E_G, m^* and ω_f are the free electron density, Fermi energy, bandgap energy, effective mass of conductive electron at the bottom of the conduction band, and angular frequency of the fundamental, respectively. From Eq.(1), one can predict that $\chi^{(3)}$ rapidly increases with smaller frequency, which indicates the strong effect of conduction band nonparabolicity on harmonic generation in the THz region. Equation (1) also shows that materials with a narrow bandgap E_G have a large effect of nonparabolicity. In this respect, indium antimonide (InSb), one of the most well-known narrow gap semiconductors (E_G =0.175 eV at room temperature [34]), is expected to have a high nonlinearity in the low frequency region. In fact, it has been reported that the four-wave mixing of the mid-infrared lights from a CO_2 laser (wavelength ~10 μm) effectively occurred in InSb [35]. However, the harmonic generation from InSb in the THz region has not been studied sufficiently. In this paper, we report our experimental study about the third harmonic generation (THG) in InSb irradiated by the output from a THz FEL. The dependence of THG intensity on the temperature and pumping intensity was investigated to understand the mechanism of THG and improve its efficiency.

The FEL at the Institute of Science and Industrial Research (SANKEN), Osaka University [11,36,37] was used as the pump beam. Fig. 1 shows the schematic experimental setup. The FEL emits 5 macro pulses per second, and each macro pulse contains ~110 of micro pulses spacing ~37 ns from each other. The central frequency of the FEL output was tuned to 4 THz (wavelength 75 μm) in this work. The path of the terahertz beam after the FEL outlet was purged by dry air to suppress the water vapor absorption. We put a 0.5 mm thick fused silica (FS) plate just after the FEL outlet to eliminate the second (8 THz) and the third (12 THz) harmonic originally contained in the FEL output [36]. Two wire grid polarizers WG_1 and WG_2 were placed after the FEL window to control the pumping beam intensity and polarization. The FEL beam is focused to a sample by a parabolic mirror. The spot size diameter was ~1.4 mm and the macropulse energy density on the sample was ~130 mJ/cm^2 unless otherwise noted. When we measured the temperature dependence of the THG, the sample was placed into a cryostat cooled by liquid nitrogen. The signal generated from the sample passed through a Michelson interferometer, and then entered the detector. We used an energy detector (Coherent, J-25MB-LE and J-10MB-LE) for pulses with energy from 300 nJ to 50 mJ, and a DLaTGS (JASCO Corp.) for weaker THG signals. To reject the residual pump beam, a cesium bromide (CsBr) crystal with a thickness of 20 mm was placed before the detector in the measurement of harmonics.

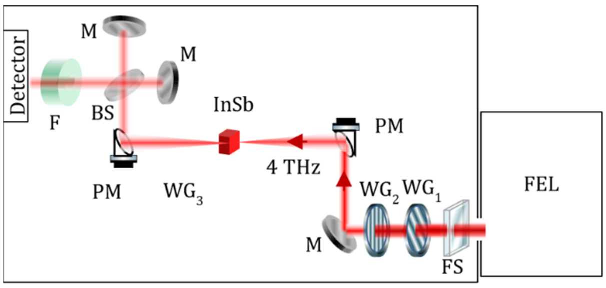

Fig. 1. Setup of the experiment. FS: fused silica; M: mirror; PM: parabolic mirror; BS: beam splitter; WG: wire grid; F: CsBr filter

An undoped InSb (100) single crystal with 430 μm thickness was used as a sample in this work. The sample was set so that one of its ⟨100⟩ axes was parallel to the polarization of the pump electric field, in which the THG was maximized. Fig. 2(a) shows the transmittance spectra of the InSb sample at 100 K and 300 K measured with a Fourier transform infrared (FT-IR) spectrometer (JASCO, FT/IR-660Plus). The overall transmittance decreases as the temperature rises due to the thermal excitation of carriers, and the transmittance at 4 THz becomes nearly zero at 300 K. It indicates that almost all the pumping beam was absorbed inside the InSb crystal or reflected at its surface at room temperature. On the other hand, the 12 THz transmittance at 300 K is high enough (~23%) for emitting the third harmonic into the direction of the pump beam incidence. The low transmittance between 5 and 6.5 THz is due to the Reststrahlen band[38], while the dips around 9.0 THz and 10.7 THz are due to the two phonon absorption [39]. To estimate the carrier density in InSb, we also measured the reflectance below 3.5 THz using a THz-time domain spectroscopy (THz-TDS) system (Advantest, TAS7500 TS), and the results at 100 K and 300 K are shown in Fig. 2(b). From the fit based on the Drude-Lorentz model[40] as discussed later, the carrier density n_e of the sample was estimated to be $\sim 4 \times 10^{14}$ and $\sim 1.2 \times 10^{16}$ cm^{-3} at 100 and 300 K, respectively. We also estimated the penetration depth at 4 THz and the coherent length of THG at 300 K to be 91 μm and 109 μm, respectively. The shorter penetration depth than the coherent length indicates that the THG efficiency in the InSb is not greatly limited by the phase mismatch.

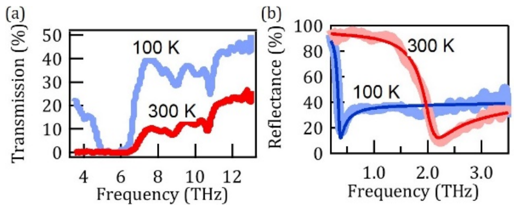

Fig. 2. (a): Transmittance of the InSb sample at 100 K (blue) and 300 K (red) from 3.5 to 13 THz. (b): Reflectance of the sample at 100 K (blue thick line) and 300 K (red thick line) from 0.2 to 3.5 THz; the accompanying thin solid lines show the fit based on the Drude-Lorentz model.

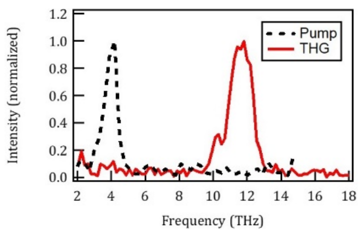

Fig. 3. Spectra of pumping beam (dashed) and generated THG signal (solid), normalized at the peak obtained at room temperature. The pumping beam and THG signal were detected with an energy detector (Coherent, J-25MB-LE) and a DLaTGS sensor, respectively.

The spectrum of the pumping beam is shown by the dashed curve in Fig. 3. The peak was located at 4 THz and its full width half maximum was around 0.8 THz. When the InSb sample was irradiated by this pumping beam at room temperature (300 K), we observed the spectrum of the solid curve in Fig. 3. A peak at around 12 THz can be seen clearly, which is the third harmonic of the pump. A small dip at ~10.7 THz is attributed to the two-phonon absorption described earlier. One can notice the absence of the second harmonic (8 THz). Note that the transmittance at 8 THz of the InSb sample (~8%) and the CsBr filter (~40%) are high enough for us to detect the second harmonic if it was generated as strongly as the third harmonic. The second harmonics was not detected even when the azimuthal angle of the sample was rotated. The nonlinear response in the THz region is attributed mainly to free electrons as described earlier, in which the even order harmonic generation is prohibited due to the centrosymmetry [41]. On the other hand, the odd order harmonic generation is allowed, and the strong nonparabolicity of the conduction band in InSb enables us to clearly observe the third harmonic.

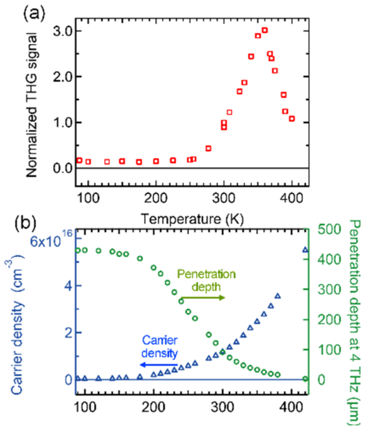

Fig. 4. (a) Temperature dependence of the third harmonic intensity normalized to that at 300 K. (b) Temperature dependence of the carrier density (triangle) and penetration depth (circle) at 4 THz estimated from the reflectance measured with THz-TDS.

Fig. 4(a) shows the THG intensity as a function of the sample temperature, normalized to the value at 300 K. When the temperature was lower than 250 K, the THG intensity was much weaker than that at 300 K, and nearly independent of the temperature. Above 250 K, the THG intensity rapidly increased with a rise in temperature. At 360 K it reached the maximum intensity of 3 times as large as that at 300 K and 22 times as large as that at 100 K. The THG power conversion efficiency at this temperature is ~1% according to the pulse energy measurement of the THG and pumping beam with an energy detector, considering the transmittance of the CsBr filter (83% at 12 THz) and the cryostat windows (cyclo-olefin polymer; 44% at 4 THz and 10% at 12 THz). This corresponds to the field conversion efficiency of 10%, which is higher than that reported for a system with topological insulator (8%) [25]. However, above 360 K the THG intensity started decreasing steeply, and at 400 K the THG intensity became again close to that at 300 K.

To understand the origin of the observed temperature dependence of the THG intensity, we estimated the temperature dependence of the carrier density and the penetration depth at 4 THz in the following way[42]: the reflectance spectra obtained by THz-TDS were fitted with the theoretical reflectance calculated from the complex dielectric function $\tilde{\epsilon}$ based on the Drude-Lorentz model appearing in [43], with the plasma frequency and electron damping constant as fitting parameters. From these results, the temperature dependence of the carrier density n_e and penetration depth at 4 THz δ_p was calculated as shown in Fig. 4(b), using an effective mass of $m^* = 0.0145m_0(1 - 5.05 \times 10^{-4}T)$ with m_0 being the free electron mass and T being the temperature [44]. This result illustrates that the significant increase of the n_e and the decrease of the δ_p simultaneously occurs around 300 K as the temperature rises. The former increases the THG efficiency because from Eq. (1) the nonlinear susceptibility is expected to be proportional to n_e. On the other hand, the latter decreases the THG efficiency because the smaller δ_p indicates that the more amount of energy of the pumping wave is dissipated as heat by linear absorption before being converted to third harmonic. The balance between these positive and negative effects determines the optimal temperature for THG, which is 360 K in the present case.

There are also other effects working together with δ_p. One effect is the Fresnel transmission at 4 THz at the entrance face of InSb, which is found to be 47 % at 100 K, reaches a maximum of 79 % at 370 K and then decreases to 75 % at 400 K. This effect may also contribute to the trend observed in Fig. 4(a). We also calculated the penetration depth at 12 THz, $\delta_p^{(12)}$, and found that it has a shape similar to δ_p in Fig. 4(b) (specifically, $\delta_p^{(12)}$ = 2400 μm at 100 K and $\delta_p^{(12)}$ = 280 μm at 360 K), which may be a small effect at low temperature, but becomes important above 360 K and contributes to the decrease of the THG intensity.

The existence of a small but nonzero temperature-independent THG at temperatures lower than 250 K may come from impurity centers: from Fig. 4b we have extracted the carrier density, a nonzero number, $\sim 4 \times 10^{14} \mathrm{cm}^{-3}$, from 80 K to 120 K. To explain why the THG is temperature independent up to 250 K, we propose that another source of carrier contributes to THG at below 250 K: the carrier due to impact ionization. The threshold electric field for impact ionization in InSb was found to be 104 kV/cm [45], while the pumping electric field in our experiment is estimated to be ~263 kV/cm, based on Ref. [15]. Thus a strong impact ionization was very likely to occur. Therefore, the THG at temperature lower than 250 K can be attributed to free carriers from impurity centers and free carriers from impact-ionization, both are temperature-independent.

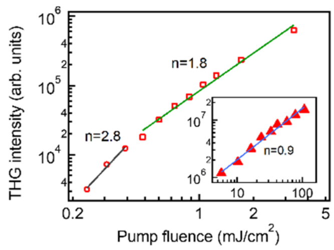

Fig. 5. THG intensity as a function of the pumping beam fluence, measured at room temperature: at low (below 0.4 mJ/cm^2, open circles), medium (0.5 to 3 mJ/cm^2, open squares) and high (above 6 mJ/cm^2, solid triangles in the inset) pump intensity region. Lines: power law fit of the experimental results. The values of "*n*" are the power law exponents of the fits associated with the data.

The dependence of the THG intensity on pump fluence below 3 mJ/cm^2 and above 6 mJ/cm^2 is shown in Fig. 5 and its inset, respectively. In the measurement below 3 mJ/cm^2, the spot diameter of the pumping beam on the sample was expanded to ~2 mm to reduce the fluence with keeping the THG signal large enough to be detected, while above 3 mJ/cm^2 the spot diameter is 1.4 mm. The fits by power law $y = Ax^n$ at three different pump intensity regions are also shown in Fig. 5: at low pumping intensity (below 0.4 mJ/cm^2, black line), the THG intensity increases following the power law with an exponent n of 2.8. This is close to $n = 3$ expected for the third order process. However, at the medium pumping intensity (0.5 to 3 mJ/cm^2, green line), the value of n decreases to 1.8. At high pump intensity (above 6 mJ/cm^2, blue line in the inset), it further decreased to only 0.9. One possible reason for the decrease of the nonlinear order n at high pumping intensity is the smaller nonparabolicity of the InSb energy band at higher energy. This can make the effective $\chi^{(3)}$ of free electrons smaller when they are more energized by the pumping wave. Another possibility is the change of refractive index in InSb depending on the pumping intensity, which is also a third order nonlinear effect [41]. This also deflects the intensity dependence of the THG from pure power law. In the case of InSb, the impact ionization [46,47] would also occur at high pumping intensity, which would also affect the intensity dependence. The saturation of the THz harmonic generation efficiency was also reported in the previous studies[26,31], in which its origin was discussed in terms of the carrier dynamics. Though the elucidation of the detailed mechanism of intensity dependence is our future challenge, it is expected that the deeper understanding on this intensity dependence will lead to a method for THG in the THz region with further high efficiencies.

In summary, we investigated THG from InSb crystal irradiated by 4 THz FEL outputs. The THG originated from non-parabolic energy band of InSb was clearly observed at 12 THz. By changing the InSb temperature, we observed that the THG signal was strongly enhanced at 360 K, 22-fold stronger than at 100 K and 3-fold stronger than at room temperature. The THG power conversion efficiency reached 1% at 360K, the highest in the THz and FIR regions below 10 THz. The dependence of THG intensity on pump intensity showed a nonlinear order smaller than 3 when the pumping intensity was strong, suggesting the potential of further improvement of the THG conversion efficiency after addressing this saturation phenomenon.

Funding. Japan Society for the Promotion of Science (JSPS) (JP20H02206, JP23K17748).

Acknowledgment. We thank Prof. M. Nagai of Osaka University for the use of his interferometer, and K. Furukawa and Y. Fukui for FEL operation. This work was performed by using the THz-FEL at Research Laboratory for Quantum Beam Science, Institute of Scientific and Industrial Research, Osaka University.

Disclosures. The authors declare no conflicts of interest.

Data availability. Data underlying the results presented in this paper are not publicly available at this time but may be obtained from the authors upon reasonable request.

Supplemental document. See Supplement for supporting content.

References

1. N. Yoshikawa, T. Tamaya, and K. Tanaka, Science **356**, 736 (2017).
2. R. Matsunaga, N. Tsuji, H. Fujita, et al., Science **345**, 1145 (2014).
3. M. Ota, K. Kan, S. Komada, et al., Nat. Phys. **18**, 1436 (2022).
4. S. Lee, S. Baek, T. Kim, et al., Adv. Mater. **32**, 2000250 (2020).
5. D. Kumar, M. Gupta, Y. K. Srivastava, et al., J. Opt. **24**, 045101 (2022).
6. Q. Wang, B. Gao, M. Raglione, et al., Laser Photonics Rev. **13**, 1900071 (2019).
7. D. Kumar, R. Jain, Shahjahan, et al., Plasmonics **15**, 1925 (2020).
8. M. Wang and E.-H. Yang, Nano-Structures & Nano-Objects **15**, 107 (2018).
9. D. Kumar, K. M. Devi, R. Kumar, et al., Opt. Commun. **491**, 126949 (2021).
10. Q. Zhou, Q. Qiu, and Z. Huang, Opt. Laser Technol. **157**, 108558 (2023).
11. K. Kawase, R. Kato, A. Irizawa, et al., Nucl. Instruments Methods Phys. Res. A **726**, 96 (2013).
12. G. Ramian, Nucl. Instruments Methods Phys. Res. A **318**, 225 (1992).
13. D. Oepts, A. F. G. van der Meer, and P. W. van Amersfoort, Infrared Phys. Technol. **36**, 297 (1995).
14. Y. U. Jeong, B. C. Lee, S. K. Kim, et al., Nucl. Instruments Methods Phys. Res. A **475**, 47 (2001).
15. M. Nagai, S. Aono, M. Ashida, et al., New J. Phys. **19**, 053017 (2017).
16. M. C. Hoffmann and J. A. Fülöp, J. Phys. D. Appl. Phys. **44**, 083001 (2011).
17. M. Hangyo, Jpn. J. Appl. Phys. **54**, 120101 (2015).
18. K. Makino, K. Kato, K. Takano, et al., Sci. Rep. **8**, 2914 (2018).
19. Y. W. Wang, S. Segawa, T. Shimizu, et al., Appl. Phys. A **128**, 836 (2022).
20. T. Kurihara, K. Hirota, H. Qiu, et al., Sci. Rep. **10**, 7231 (2020).
21. G. Fitzky, M. Nakajima, Y. Koike, et al., Phys. Rev. Lett. **127**, 107401 (2021).
22. M. J. Farrar, F. W. Wise, J. R. Fetcho, et al., Biophys. J. **100**, 1362 (2011).
23. G. Ramos-Ortiz, M. Cha, S. Thayumanavan, et al., Appl. Phys. Lett. **85**, 179 (2004).
24. M. R. Siegrist, F. Keilmann, C. Nieswand, et al., Infrared Phys. Technol. **36**, 407 (1995).
25. K. J. Tielrooij, A. Principi, D. S. Reig, et al., Light Sci. Appl. **11**, 315 (2022).
26. H. A. Hafez, S. Kovalev, J. C. Deinert, et al., Nature **561**, 507 (2018).
27. D. N. Gupta, Plasmonics **16**, 419 (2021).
28. T. N. K. Phan, K. Kato, G. Isoyama, et al., in *43rd Int. Conf. Infrared, Millimeter, Terahertz Waves* (2018), p. 8509972.
29. M. Nakajima, S. Ueda, K. Kato, et al., in *45th Int. Conf. Infrared, Millimeter, Terahertz Waves* (2020), p. 9370493.
30. T. A. Uaman Svetikova, T. V. A. G. A. G. de Oliveira, A. Pashkin, et al., ACS Photonics **10**, 3708 (2023).
31. F. Meng, F. Walla, S. Kovalev, et al., Phys. Rev. Res. **5**, 043141 (2023).
32. F. Meng, M. D. Thomson, Q. Ul-Islam, et al., Phys. Rev. B **102**, 075205 (2020).
33. P. A. Wolff and G. A. Pearson, Phys. Rev. Lett. **17**, 1015 (1966).
34. E. O. Kane, J. Phys. Chem. Solids **1**, 249 (1957).
35. C. K. N. Patel, R. E. Slusher, and P. A. Fleury, Phys. Rev. Lett. **17**, 1011 (1966).
36. R. Kato, R. A. V. Kumar, M. Kuwahara, et al., Nucl. Instruments Methods Phys. Res. Sect. A Accel. Spectrometers, Detect. Assoc. Equip. **483**, 46 (2002).
37. G. Isoyama, JAS4QoL **6**, 2 (2020).
38. D. J. Lockwood, G. Yu, and N. L. Rowell, Solid State Commun. **136**, 404 (2005).
39. E. S. Koteles, W. R. Datars, and G. Dolling, Phys. Rev. B **9**, 572 (1974).
40. V. C. Agulto, K. Toya, T. N. K. Phan, et al., Appl. Phys. Lett. **118**, 42101 (2021).
41. R. W. Boyd, Nonlinear Optics, Third Ed. (Academic Press, 2008).
42. R. A. Lewis, Terahertz Physics (Cambridge University Press, 2013).
43. R. T. Holm, in *Handbook of Optical Constants of Solids*, E. D. Palik, ed. (Academic Press, 1985), pp. 491–502.
44. R. W. Cunningham and J. B. Gruber, J. Appl. Phys. **41**, 1804 (1970).
45. M. C. Hoffmann, J. Hebling, H. Y. Hwang, et al., J. Opt. Soc. Am. B **26**, 29 (2009).
46. C. L. Dick Jr. and B. Ancker-Johnson, Phys. Rev. B **5**, 526 (1972).
47. M. C. Hoffmann, J. Hebling, H. Y. Hwang, et al., Phys. Rev. B **79**, 161201 (2009).

References with article titles

1. N. Yoshikawa, T. Tamaya, and K. Tanaka,"High-harmonic generation in graphene enhanced by elliptically polarized light excitation," Science **356**, 736 (2017).
2. R. Matsunaga, N. Tsuji, H. Fujita, A. Sugioka, K. Makise, Y. Uzawa, H. Terai, Z. Wang, H. Aoki, and R. Shimano,"Light-induced collective pseudospin precession resonating with Higgs mode in a superconductor," Science **345**, 1145 (2014).
3. M. Ota, K. Kan, S. Komada, Y. Wang, V. C. Agulto, V. K. Mag-usara, Y. Arikawa, M. R. Asakawa, Y. Sakawa, T. Matsui, and M. Nakajima,"Ultrafast visualization of an electric field under the Lorentz transformation," Nat. Phys. **18**, 1436 (2022).
4. S. Lee, S. Baek, T. Kim, H. Cho, S. Lee, J. Kang, and B. Min,"Metamaterials for Enhanced Optical Responses and their Application to Active Control of Terahertz Waves," Adv. Mater. **32**, 2000250 (2020).
5. D. Kumar, M. Gupta, Y. K. Srivastava, K. M. Devi, R. Kumar, and D. Roy Chowdhury,"Photoinduced dynamic tailoring of near-field coupled terahertz metasurfaces and its effect on Coulomb parameters," J. Opt. **24**, 045101 (2022).
6. Q. Wang, B. Gao, M. Raglione, H. Wang, B. Li, F. Toor, M. A. Arnold, and H. Ding,"Design, Fabrication, and Modulation of THz Bandpass Metamaterials," Laser Photonics Rev. **13**, 1900071 (2019).
7. D. Kumar, R. Jain, Shahjahan, S. Banerjee, S. S. Prabhu, R. Kumar, A. K. Azad, and D. Roy Chowdhury,"Bandwidth Enhancement of Planar Terahertz Metasurfaces via Overlapping of Dipolar Modes," Plasmonics **15**, 1925 (2020).
8. M. Wang and E.-H. Yang,"THz applications of 2D materials: Graphene and beyond," Nano-Structures & Nano-Objects **15**, 107 (2018).
9. D. Kumar, K. M. Devi, R. Kumar, and D. Roy Chowdhury,"Dynamically tunable slow light characteristics in graphene based terahertz metasurfaces," Opt. Commun. **491**, 126949 (2021).
10. Q. Zhou, Q. Qiu, and Z. Huang,"Graphene-based terahertz optoelectronics," Opt. Laser Technol. **157**, 108558 (2023).
11. K. Kawase, R. Kato, A. Irizawa, M. Fujimoto, S. Kashiwagi, S. Yamamoto, F. Kamitsukasa, H. Osumi, M. Yaguchi, A. Tokuchi, S. Suemine, and G. Isoyama,"The high-power operation of a terahertz free-electron laser based on a normal conducting RF linac using beam conditioning," Nucl. Instruments Methods Phys. Res. A **726**, 96 (2013).
12. G. Ramian,"The new UCSB free-electron lasers," Nucl. Instruments Methods Phys. Res. A **318**, 225 (1992).
13. D. Oepts, A. F. G. van der Meer, and P. W. van Amersfoort,"The Free-Electron-Laser user facility FELIX," Infrared Phys. Technol. **36**, 297 (1995).
14. Y. U. Jeong, B. C. Lee, S. K. Kim, S. O. Cho, B. H. Cha, J. Lee, G. M. Kazakevitch, P. D. Vobly, N. G. Gavrilov, V. V Kubarev, and G. N. Kulipanov,"First lasing of the KAERI compact far-infrared free-electron laser driven by a magnetron-based microtron," Nucl. Instruments Methods Phys. Res. A **475**, 47 (2001).
15. M. Nagai, S. Aono, M. Ashida, K. Kawase, A. Irizawa, and G. Isoyama,"Luminescence induced by electrons outside zinc oxide nanoparticles driven by intense terahertz pulse trains," New J. Phys. **19**, 053017 (2017).
16. M. C. Hoffmann and J. A. Fülöp,"Intense ultrashort terahertz pulses: generation and applications," J. Phys. D. Appl. Phys. **44**, 083001 (2011).
17. M. Hangyo,"Development and future prospects of terahertz technology," Jpn. J. Appl. Phys. **54**, 120101 (2015).
18. K. Makino, K. Kato, K. Takano, Y. Saito, J. Tominaga, T. Nakano, G. Isoyama, and M. Nakajima,"Significant Volume Expansion as a Precursor to Ablation and Micropattern Formation in Phase Change Material Induced by Intense Terahertz Pulses," Sci. Rep. **8**, 2914 (2018).
19. Y. W. Wang, S. Segawa, T. Shimizu, V. C. Agulto, V. K. Mag-usara, K. Kato, K. Miyamoto, T. Omatsu, K. Makino, J. Tominaga, G. Isoyama, M. Asakawa, and M. Nakajima,"Ablation phenomena by intense terahertz vortex beam," Appl. Phys. A **128**, 836 (2022).
20. T. Kurihara, K. Hirota, H. Qiu, K. T. N. Phan, K. Kato, G. Isoyama, and M. Nakajima,"Reconfiguration of magnetic domain structures of $ErFeO_3$ by intense terahertz free electron laser pulses," Sci. Rep. **10**, 7231 (2020).
21. G. Fitzky, M. Nakajima, Y. Koike, A. Leitenstorfer, and T. Kurihara,"Ultrafast Control of Magnetic Anisotropy by Resonant Excitation of 4f Electrons and Phonons in $Sm_{0.7}Er_{0.3}FeO_3$," Phys. Rev. Lett. **127**, 107401 (2021).
22. M. J. Farrar, F. W. Wise, J. R. Fetcho, and C. B. Schaffer,"In vivo imaging of myelin in the vertebrate central nervous system using third harmonic generation microscopy.," Biophys. J. **100**, 1362 (2011).
23. G. Ramos-Ortiz, M. Cha, S. Thayumanavan, J. C. Mendez, S. R. Marder, and B. Kippelen,"Third-order optical autocorrelator for time-domain operationat telecommunication wavelengths," Appl. Phys. Lett. **85**, 179 (2004).
24. M. R. Siegrist, F. Keilmann, C. Nieswand, and M. Urban,"Far-infrared wave generation by frequency tripling," Infrared Phys. Technol. **36**, 407 (1995).
25. K. J. Tielrooij, A. Principi, D. S. Reig, A. Block, S. Varghese, S. Schreyeck, K. Brunner, G. Karczewski, I. Ilyakov, O. Ponomaryov, T. V. A. G. de Oliveira, M. Chen, J. C. Deinert, C. G. Carbonell, S. O. Valenzuela, L. W. Molenkamp, T. Kiessling, G. V. Astakhov, and S. Kovalev,"Milliwatt terahertz harmonic generation from topological insulator metamaterials," Light Sci. Appl. **11**, 315 (2022).
26. H. A. Hafez, S. Kovalev, J. C. Deinert, Z. Mics, B. Green, N. Awari, M. Chen, S. Germanskiy, U. Lehnert, J. Teichert, Z. Wang, K. J. Tielrooij, Z. Liu, Z. Chen, A. Narita, K. Müllen, M. Bonn, M. Gensch, and D. Turchinovich,"Extremely efficient terahertz high-harmonic generation in graphene by hot Dirac fermions," Nature **561**, 507 (2018).
27. D. N. Gupta,"Optical Second-Harmonic Generation of Terahertz Field from n-type InSb Semiconductors," Plasmonics **16**, 419 (2021).
28. T. N. K. Phan, K. Kato, G. Isoyama, M. Yoshimura, S. Fujioka, and M. Nakajima,"Third harmonic generation from InSb excited by Free Electron Laser," in *43rd Int. Conf. Infrared, Millimeter, Terahertz Waves* (2018), p. 8509972.
29. M. Nakajima, S. Ueda, K. Kato, T. N. K. Phan, T. Shimizu, M. Tani, and M. Yoshimura,"Study of harmonic generation from InSb excited by terahertz wave pulses with femtosecond pulse laser excitation," in *45th Int. Conf. Infrared, Millimeter, Terahertz Waves* (2020), p. 9370493.
30. T. A. Uaman Svetikova, T. V. A. G. A. G. de Oliveira, A. Pashkin, A. Ponomaryov, C. Berger, L. Fürst, F. B. Bayer, E. G. Novik, H. Buhmann, L. W. Molenkamp, M. Helm, T. Kiessling, S. Winnerl, S. Kovalev, and G. V. Astakhov,"Giant THz Nonlinearity in Topological and Trivial HgTe-Based Heterostructures," ACS Photonics **10**, 3708 (2023).
31. F. Meng, F. Walla, S. Kovalev, J.-C. Deinert, I. Ilyakov, M. Chen, A. Ponomaryov, S. G. Pavlov, H.-W. Hübers, N. V. Abrosimov, C. Jungemann, H. G. Roskos, and M. D. Thomson,"Higher-harmonic generation in boron-doped silicon from band carriers and bound-dopant photoionization," Phys. Rev. Res. **5**, 043141 (2023).
32. F. Meng, M. D. Thomson, Q. Ul-Islam, B. Klug, A. Pashkin, H. Schneider, and H. G. Roskos,"Intracavity third-harmonic generation in Si:B pumped by intense terahertz pulses," Phys. Rev. B **102**, 075205 (2020).
33. P. A. Wolff and G. A. Pearson,"Theory of Optical Mixing by Mobile Carriers in Semiconductors," Phys. Rev. Lett. **17**, 1015 (1966).
34. E. O. Kane,"Band structure of indium antimonide," J. Phys. Chem. Solids **1**, 249 (1957).

35. C. K. N. Patel, R. E. Slusher, and P. A. Fleury,"Optical Nonlinearities due to Mobile Carriers in Semiconductors," Phys. Rev. Lett. **17**, 1011 (1966).
36. R. Kato, R. A. V. Kumar, M. Kuwahara, M. Fujimoto, Y. Nakamura, T. Igo, T. Konishi, S. Isaka, S. Mitani, S. Okuda, S. Suemine, and G. Isoyama,"Higher harmonic generation observed in SASE in the far-infrared region," Nucl. Instruments Methods Phys. Res. Sect. A Accel. Spectrometers, Detect. Assoc. Equip. **483**, 46 (2002).
37. G. Isoyama,"Development of a Free-Electron Laser in the Terahertz Region," JAS4QoL **6**, 2 (2020).
38. D. J. Lockwood, G. Yu, and N. L. Rowell,"Optical phonon frequencies and damping in AlAs, GaP, GaAs, InP, InAs and InSb studied by oblique incidence infrared spectroscopy," Solid State Commun. **136**, 404 (2005).
39. E. S. Koteles, W. R. Datars, and G. Dolling,"Far-infrared phonon absorption in InSb," Phys. Rev. B **9**, 572 (1974).
40. V. C. Agulto, K. Toya, T. N. K. Phan, V. K. Mag-Usara, J. Li, M. J. F. Empizo, T. Iwamoto, K. Goto, H. Murakami, Y. Kumagai, N. Sarukura, M. Yoshimura, and M. Nakajima,"Anisotropic complex refractive index of β-Ga_2O_3 bulk and epilayer evaluated by terahertz time-domain spectroscopy," Appl. Phys. Lett. **118**, 42101 (2021).
41. R. W. Boyd,"Nonlinear Optics," Third Ed. (Academic Press, 2008).
42. R. A. Lewis,"Terahertz Physics," (Cambridge University Press, 2013).
43. R. T. Holm,"InSb," in *Handbook of Optical Constants of Solids*, E. D. Palik, ed. (Academic Press, 1985), pp. 491–502.
44. R. W. Cunningham and J. B. Gruber,"Intrinsic Concentration and Heavy-Hole Mass in InSb," J. Appl. Phys. **41**, 1804 (1970).
45. M. C. Hoffmann, J. Hebling, H. Y. Hwang, K. Yeh, and K. A. Nelson,"THz-pump/THz-probe spectroscopy of semiconductors at high field strengths [Invited]," J. Opt. Soc. Am. B **26**, 29 (2009).
46. C. L. Dick Jr. and B. Ancker-Johnson,"Nonequilibrium Carrier Phenomena in *n*-Type InSb," Phys. Rev. B **5**, 526 (1972).
47. M. C. Hoffmann, J. Hebling, H. Y. Hwang, K.-L. Yeh, and K. A. Nelson,"Impact ionization in InSb probed by terahertz pump—terahertz probe spectroscopy," Phys. Rev. B **79**, 161201 (2009).